Control Engineering Practice 170 (2026) 106835

Contents lists available at ScienceDirect

Control Engineering Practice

journal homepage: www.elsevier.com/locate/conengprac

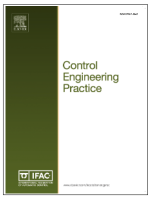

Experimental evaluation of extremum seeking control in semi-industrial microalgae raceway ponds

José González-Hernández [a,*], Laurent Dewasme [b], José Luis Guzmán [a], José Carlos Moreno [a], Alain Vande Wouwer [b]

[a] Department of Informatics, University of Almería, CIESOL, ceiA3, La Cañada de San Urbano s/n, Almería, Spain
[b] Systems, Estimation, Control and Optimization (SECO), University of Mons, Mons, B-7000, Belgium

ARTICLE INFO

Keywords:
Real-time optimization
Process control
Extremum seeking control
Microalgae
Raceway pond

ABSTRACT

This work presents the implementation and experimental evaluation of an extremum seeking control (ESC) strategy for pH regulation in semi-industrial microalgae raceway photobioreactors, where pH is one of the most critical variables to control for ensuring stable and productive operation. A model-free optimization approach is proposed based on the classical modulation-demodulation ESC scheme, particularly suited to bioreactors whose dynamics evolve slowly and vary over time due to irradiance, temperature, mixing and biomass growth. To enable within-day convergence, the dither frequency was deliberately placed outside the dominant bandwidth of the process, ensuring sufficient excitation cycles during daylight operation. The high-pass filter (HPF) cutoff was then tuned to reject slow diurnal drifts while providing the phase lead required by the out-of-band design, thus preserving an accurate gradient estimate. In addition, a static data-driven feedforward of solar irradiance was incorporated to cancel predictable disturbances associated with photosynthetic activity, improving transient response and reducing corrective effort from the ESC loop. The approach was deployed on full-scale 80 m^2 raceways under realistic outdoor and semi-industrial conditions. Results demonstrate robust pH regulation and fast daytime convergence toward the optimal operating region, with minimal modelling effort, highlighting ESC as a practical and effective tool for real-time pH control in microalgal bioprocesses.

1. Introduction

Microalgae are photosynthetic microorganisms that have attracted increasing interest in recent years because of their potential to address environmental and food-related challenges (Acién et al., 2012). Their rapid growth in a wide variety of environments (Tapie & Bernard, 1988) and their ability to remove pollutants and nutrients from wastewater (Nordio et al., 2022) make them a promising basis for sustainable processes. During growth, microalgae also capture carbon dioxide (CO_2) and convert it into biomass, thereby contributing to climate-change mitigation through net greenhouse-gas removal.

Microalgae are typically cultivated in photobioreactors, which are broadly classified as open or closed systems. Open reactors make direct use of sunlight and are suitable for large-scale production, but they pose challenges for contamination control and harvesting efficiency. Closed reactors, including tubular and columnar designs, provide tighter control of cultivation conditions and thus facilitate optimization of productivity and biomass quality. The choice between these configurations depends mainly on production scale and application targets.

For wastewater treatment and for biomass production not intended for food or pharmaceutical use, open *raceway* reactors are the dominant industrial technology for microalgae cultivation (Acién et al., 2017; Johnson et al., 1988). These oval-loop systems with continuous circulation offer high throughput at low cost. However, their optimal operation is intrinsically tied to weather conditions, since providing artificial illumination and temperature control at this scale is economically unfeasible (González-Hernández et al., 2022).

The microalgal growth rate depends mainly on solar radiation, temperature, pH, dissolved oxygen, and nutrient availability (Sánchez-Zurano et al., 2021). The pH is usually regulated by injecting CO_2, which acidifies the culture while supplying inorganic carbon; as a result, pH control has received considerable attention in recent years (Carreño Zagarra et al., 2019; Pawlowski et al., 2019; Rodríguez-Miranda et al., 2019). Dissolved oxygen can be managed by aeration, which strips

---

[*] Corresponding author.

E-mail addresses: j.gonzalez@ual.es (J. González-Hernández), Laurent.DEWASME@umons.ac.be (L. Dewasme), joseluis.guzman@ual.es (J.L. Guzmán), jcmoreno@ual.es (J.C. Moreno), alain.vandewouwer@umons.ac.be (A. Vande Wouwer).

https://doi.org/10.1016/j.conengprac.2026.106835
Received 25 November 2025; Received in revised form 12 January 2026; Accepted 4 February 2026

oxygen from the medium. Nutrients are seldom limiting in wastewater, and when fresh water or agricultural effluents are used, nutrient levels can be corrected by fertilizer addition. In practice, radiation and culture temperature remain the only major factors that cannot be directly or economically controlled.

Among the previous variables, pH control is the most critical one to be controlled due to its continuous varying dynamics, and its direct connection with the microalgae photosynthesis rate and weather conditions (Guzmán et al., 2025). For this reason, prior work on pH regulation in raceway photobioreactors largely relies on explicit or learned models combined with frequent retuning, where it was demonstrated that the pH dynamics is locally stable. Classical PI loops depend on process characterization and must be periodically re-identified as conditions drift. Hybrid MRAC and relay-based PI autotuning can accommodate slow seasonal changes, but they still assume fixed controller structures and require dedicated excitation campaigns (Caparroz et al., 2025a,b). Data-driven surrogates wrapped around PI provide adaptability at the cost of curating and refreshing large datasets (Caparroz et al., 2024), while day/night switching and event-based logic remain tied to offline tuning and fixed setpoints (Rodríguez-Miranda et al., 2020). Learning-based MPC achieves strong regulation by maintaining a predictive model update online (Pataro et al., 2023). Recently, another MPC-based approach has been reported, where a model-on-demand strategy is adopted to account for the changing system dynamics by constructing local ARX models from an online regressor database (Otálora et al., 2026). In outdoor raceways, however, slow recirculation, large transport delays, and strong diurnal forcing make model identification and maintenance costly and fragile, as key process characteristics such as biomass concentration, contamination, and culture adaptation evolve over time. These limitations motivate the use of a model-free strategy that can directly exploit measurements without relying on a maintained and updated process model.

Extremum seeking control (ESC) provides such a strategy, where by injecting a small periodic dither and demodulating the measured performance, the controller estimates the local gradient online and steers the operating point toward the pH that maximizes a chosen objective, without requiring an explicit process model and while naturally adapting to time-varying dynamics (Ariyur & Krstić, 2003; Krstić & Wang, 2000; Tan et al., 2006). Former applications include real-time autotuning and optimization in power systems, combustion, fluid dynamics, and bioprocesses (Dewasme & Vande Wouwer, 2020), including lab-scale photobioreactors (Feudjio Letchindjio et al., 2019, 2021; Lara et al., 2025). Most of these studies address comparatively fast systems, where the large number of dither cycles per unit time enables rapid gradient estimation and convergence, although ESC has also been successfully applied to slower bioprocesses. In contrast, the raceway considered in this work exhibits slow dynamics and long delays and is further constrained by a limited optimization window, because no control action can be applied at night due to the inversion of the reactor dynamics. Notice that, as reviewed above, this system has already been regulated with multiple alternative pH control strategies. However, the aim of this work is not to introduce another controller or benchmark ESC against existing methods, but to show that an ESC loop can be deployed, tuned, and operated reliably under the demanding conditions of a semi-industrial outdoor raceway. The main contribution lies in the successful experimental evaluation of ESC, demonstrating its practical viability in a setting where model-based strategies are fragile and where real-time, measurement-driven optimization is particularly valuable.

To this end, we deploy an ESC architecture on an outdoor 80 m^2 raceway and augment it with plant-ready features (daylight gate and short warm-up, static irradiance feedforward, discrete demodulation with explicit phase lead, slew-limited integrator with guard-banded saturation, and a small positive lower bound on CO_2 flow) to secure within-day convergence and robust tracking under strong irradiance fluctuations, keeping the real reactor close to its optimal pH across changing culture states. Notice that, before field deployment, the proposed ESC strategy was first evaluated in simulation using a nonlinear dynamic model of the raceway. This allowed us to assess convergence speed, robustness to diurnal forcing, and sensitivity to operating conditions by subjecting the virtual reactor to a wide range of irradiance profiles, biomass concentrations, and hydrodynamic regimes. These tests provided the necessary insights to select feasible dither frequencies, verify the adequacy of the gradient-estimation filters, and define safe actuator limits prior to implementation. To the best of our knowledge, this constitutes the first semi-industrial scale validation of an ESC strategy in a raceway photobioreactor.

This paper is structured as follows. Section 2 is devoted to summarize the raceway model used for simulation purposes, the real raceway reactor used for experimental evaluation, and the basis of the classical ESC approach. In Section 3, the main results of this work are described. First, tuning and modification of the classical ESC scheme for the pH regulation control problem are presented in relation to dither placement and tuning, phase lag and transport delay, feedforward capabilities, and discrete-time realization. After that, the proposed control scheme is evaluated in simulation for tuning and analysis purposes, and then experimental trials are presented to show the successful deployment of the ESC strategy in the real reactor. Section 4 is dedicated to analyzing the results obtained and the conclusions are depicted in Section 5.

2. Materials and methods

2.1. Raceway simulator

In this work, a nonlinear dynamic model of the raceway photobioreactor is employed to conduct a preliminary analysis of the ESC strategy and to extract qualitative insights regarding its tuning. It is important to emphasize that the model is used exclusively for simulation analysis and not for controller design. Due to its structural complexity, strong nonlinearities, and dependence on time-varying biological parameters, such a model would require continuous recalibration to remain predictive, making it impractical as a basis for real-time control synthesis. Nonetheless, the model remains highly valuable in the analysis phase: it captures the dominant hydrodynamic, biochemical, and radiative dynamics of the process, enabling systematic exploration of operating conditions, perturbation profiles, and ESC tuning choices before field deployment.

The most important dynamical components of the model are summarized the following sections, where the mathematical foundation follows the formulation proposed by Guzmán et al. (2025). The architecture comprises two interconnected blocks: *biological model*, which computes the microalgal growth rate, and *dynamic model*, which solves the mass and energy balances of the photobioreactor, including carbon and oxygen fluxes and heat exchanges between different zones of the culture. The simulator is freely available in Rodríguez Miranda et al. (2025).

2.1.1. Biological model

Biomass production is quantified through the specific growth rate μ, which depends on the average available irradiance (I_{av}), temperature (T), pH, dissolved oxygen concentration (O_2), and microbial respiration (m). Following (Sánchez-Zurano et al., 2021), a light-dependent term $\mu(I_{av})$ is weighted by three dimensionless factors $\overline{\mu(\cdot)} \in [0,1]$ capturing the effects of T, pH, and O_2, while assuming non-limiting nutrients (N, P, etc.):

$$\mu = \mu(I_{av})\,\overline{\mu(T)}\,\overline{\mu(pH)}\,\overline{\mu(O_2)} - m. \tag{1}$$

where $\mu_{(I_{av})}$ is the maximum specific growth rate attainable by the culture as a function of the mean irradiance and $\overline{\mu(\cdot)} \in [0,1]$ is a dimensionless allocation factor accounting for the fraction of gross photosynthesis effectively converted into specific growth rate. Such multiplicative structures are common in dynamic microalgae models for raceways and closed. For a more detailed information see (Rodríguez-Miranda et al., 2025; Sánchez-Zurano et al., 2021).

2.1.2. Dynamic model

The reactor is modeled as a perfectly mixed tank. The main state variables, biomass (C_b), dissolved oxygen ($[O_2]$), and total inorganic carbon ($[C_T]$), evolve according to the following ordinary differential equations:

$$\frac{dC_b}{dt} = C_b\left(\mu - d_r - \frac{Q_d}{V_r}\right) \tag{2}$$

$$\begin{aligned}\frac{d[O_2]}{dt} &= \frac{Q_d}{V_r}\left([O_2^*] - [O_2]\right) + \mu\,\frac{Y_{O_2}}{M_{O_2}}\,C_b \\ &\quad + K^{\text{atm}}_{laO_2}\left([O_2^*] - [O_2]\right) + K_{laO_2}\left([O_2^{\text{iny}}] - [O_2]\right)\end{aligned} \tag{3}$$

$$\begin{aligned}\frac{d[C_T]}{dt} &= \frac{Q_d}{V_r}\left([C_{T\text{in}}] - [C_T]\right) - \mu\,\frac{Y_{CO_2}}{M_{CO_2}}\,C_b \\ &\quad + K^{\text{atm}}_{laCO_2}\left([CO_2^*] - [CO_2]\right) + K_{laCO_2}\left([CO_2^{\text{iny}}] - [CO_2]\right)\end{aligned} \tag{4}$$

where the model inputs are the dilution flow rate Q_d, the oxygen injection flow rate O_2^{iny} (supplied from air), and the carbon dioxide injection flow rate CO_2^{iny}. All model parameters and units are summarized in Table Table A.1 of Appendix A.

Eq. (2) combines cellular production, cell death (d_r), and the dilution effect (Q_d/V_r). In Eq. (3), the dynamics of $[O_2]$ arise from dilution, photosynthesis (where Y_{O_2}/M_{O_2} converts grams of biomass to moles of oxygen), gas transfer with the atmosphere ($K^{\text{atm}}_{laO_2}$), and forced aeration (K_{laO_2}). The carbon balance Eq. (4) is analogous, but the photosynthetic term appears with the opposite sign, reflecting CO_2 consumption. In both gases, interphase exchange fluxes are governed by the volumetric mass-transfer coefficients K_{la} and the deviation from saturation equilibrium. More information about the full model can be found in Guzmán et al. (2025), Rodríguez Miranda et al. (2025).

2.2. Raceway reactor

To evaluate performance under real operating conditions, a raceway photobioreactor belonging to the CIESOL research center from the Universtiy of Almería and located at IFAPA facilities (Almería, Spain). The raceway consists of two 40 m channels connected at their ends by a U-shaped bend. Each channel is 1 m wide with a maximum depth of 30 cm; the usual operating depth is 10–15 cm, with an optimal operating height around 0.15 m (González-Hernández et al., 2022). This configuration yields a total surface area of 80 m^2, corresponding to a volume-depth ratio of 800 $\text{L}\,\text{cm}^{-1}$. The reactor is installed outdoors (Fig. 1) and captures real dynamics closer to those found in industrial facilities.

The raceway reactors are managed by a Schneider Modicon M241 PLC, which integrates an OPC UA server for data exchange. Through this interface, sensor measurements are acquired and actuator commands are issued. In the present work, the relevant measurements are the pH value, obtained from a Crison 50 10 T probe, and the global solar irradiance, measured using a Kipp & Zonen CM 6B pyranometer.

The manipulated variable is the CO_2 injection flow rate, which is regulated by a FESTO VEMD proportional valve equipped with an internal control loop that allows operation through a flow-rate setpoint. All process data are transmitted via Ethernet to an industrial switch, making them accessible to other PLCs and supervisory computers within the facility.

In this study, a desktop computer running MATLAB is used to implement the proposed ESC algorithm. A MATLAB script executes read-compute-write loop by communicating with the OPC UA server, acquiring sensor data, computing the control action, and updating the CO_2 flow setpoint. This control cycle is executed with a fixed sampling time of 1 min.

Fig. 1. 80 m^2 outdoor *raceway* reactor at the IFAPA center.

2.3. Extremum-seeking control (ESC)

ESC addresses the real-time optimization of a scalar performance index using only plant measurements, without requiring an explicit model of the underlying process dynamics. Let $y(t) \in \mathbb{R}$ denote the measured process output. The closed-loop performance is quantified through an instantaneous cost function

$$J(t) = \Psi\big(y(t)\big),$$

where $\Psi(\cdot)$ maps the current process measurements to the objective of interest (e.g., productivity, efficiency, or deviation from a desired operating condition). In contrast to steady-state formulations, ESC treats $J(t)$ as a dynamic signal containing both the slow variations of the underlying process and the fast perturbations induced by the controller.

A classical modulation-demodulation ESC scheme is used to optimize in real time the performance index $J(t)$ computed from these measurements. The controller injects a small sinusoidal perturbation (“dither”) of angular frequency ω_d into the manipulated variable, demodulates the resulting performance signal using the same reference, and integrates a scaled estimate of the local gradient to drive the operating point toward an extremum (Ariyur & Krstić, 2003; Krstić & Wang, 2000; Tan et al., 2006). Fig. 2 shows the canonical structure corresponding to this implementation.

For a single decision variable, a standard ESC realization consistent with Fig. 2 is

$$u = \hat{\theta} + a\,\sin(\omega_d t), \tag{5}$$

$$\dot{\hat{\theta}} = k\,\hat{\xi}, \tag{6}$$

$$\dot{\hat{\xi}} = -\omega_l \hat{\xi} + \omega_l (J - \eta)\,a\,\sin(\omega_d t), \tag{7}$$

$$\dot{\eta} = -\omega_h \eta + \omega_h J. \tag{8}$$

The ESC dynamics in the previous equations can be interpreted as follows. The signal $u = \hat{\theta} + a\sin(\omega_d t)$ in Eq. (5) is obtained by adding a sinusoidal dither of amplitude a and frequency ω_d to the slowly varying

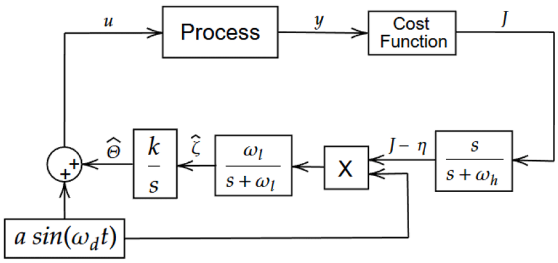

Fig. 2. Classical modulation–demodulation ESC: a sinusoidal dither $a\sin(\omega_d t)$ is summed with the input. The process output is mapped to a cost J, high-pass filtered (washout $s/(s+\omega_h)$), multiplied by the reference dither (block X), low-pass filtered $(\omega_l/(s+\omega_l))$, and finally integrated with gain k/s to update the operating point.

estimate $\hat{\theta}$. The cost signal J is processed by a first-order high-pass filter whose state-space realization is given by Eq. (8) together with the subtraction $J-\eta$. In this realization, Eq. (8) acts as a low-pass filter on J, producing the slowly varying component η, and the high-pass output is obtained as $J-\eta$. This removes the constant and slowly varying part of J and isolates the component induced by the injected dither. Multiplication of $J-\eta$ by $a\sin(\omega_d t)$ demodulates this component and produces a local estimate of the gradient direction. The low-pass filter in Eq. (7) then rejects the oscillatory terms, resulting in the smooth gradient estimate $\hat{\zeta}$, which is integrated in Eq. (6) to update the parameter $\hat{\theta}$. In this classical ESC scheme the tuning parameters are the dither amplitude a, the dither frequency ω_d, the cutoff frequencies ω_h and ω_l of the filters, and the integrator gain k.

3. ESC for pH regulation in raceway reactors

This section evaluates the proposed ESC strategy for daytime pH regulation in raceway photobioreactors under real operating conditions. Within a single, coherent workflow, the tuning of an out-of-band dither is detailed to guarantee convergence within the daylight window; the phase lag at the dither frequency is counteracted by a high-pass (washout) lead with explicit treatment of transport delay; and irradiance feedforward is incorporated to improve disturbance rejection by anticipating predictable diurnal forcing. The final controller architecture is summarized, including the practical need for a discrete-time realization for deployment.

In the context of raceway photobioreactors, the ESC framework can be directly applied to regulate the culture pH, which is one of the most sensitive variables affecting photosynthetic activity, CO_2 availability, and overall biomass productivity. Here, the manipulated variable $u(t)$ corresponds to the CO_2 injection rate, and the measured output $y(t)$ is the culture pH. A suitable performance function can therefore be defined as

$$J(t) = 1 - \left(\frac{pH(t) - pH^{\star}}{2}\right)^2, \tag{9}$$

where $pH^{\star}$ denotes the productivity-maximizing operating point for the microalgae being produced in the reactor. This choice penalizes deviations from the optimal pH and attains its maximum when the reactor operates at $y(t) = pH^{\star}$. More generally, $\Psi(\cdot)$ may incorporate additional measurements (e.g., alkalinity, dissolved oxygen, or irradiance) to reflect productivity or carbon-utilization efficiency. With this formulation, the ESC loop adjusts the CO_2 flow to maximize $J(t)$ in real time, enabling the reactor to track the optimal pH despite slow biomass-driven drifts, diurnal forcing, and long hydraulic delays inherent to outdoor raceways.

Fig. 3 summarizes the final continuous-time ESC structure implemented in this work that includes classical modulation-demodulation with an out-of-band dither, a washout tuned for phase lead/centering, demodulation delayed by the measured transport time, and no explicit low-pass (the integrator provides averaging), slew limiter and anti-windup. Application-specific additions preserve the informative content of the excitation and respect actuator constraints.

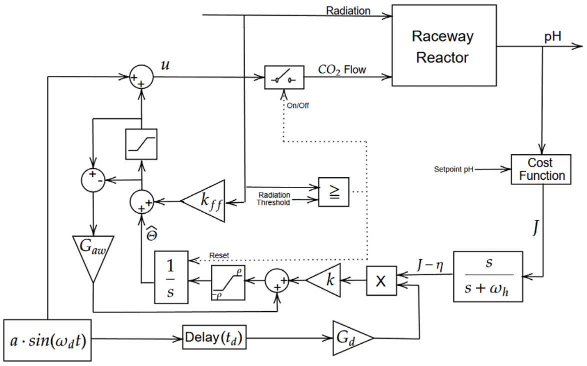

Fig. 3. Final continuous-time ESC with transport-delay demodulation, washout lead, *slew-limited* integrator, guard-banded saturation, anti-windup (back-calculation), and daily integrator reset.

In this architecture, the main ESC tuning parameters inherited from the classical scheme are the dither amplitude a, the dither frequency ω_d, the high-pass cutoff ω_h, and the adaptation gain k. The additional blocks introduce application-specific tuning knobs: the demodulation signal gain G_d and the explicit delay block t_d determine the amplitude and phase of the demodulating signal at ω_d; the gain k_{ff} sets the magnitude of the radiation-based feedforward contribution that defines the nominal CO_2 flow around which ESC operates; the slew limited values ρ restricts the slope at the integrator output, ensuring that the dither is not distorted; and the gain G_{aw} specifies the strength of the anti-windup feedback from the actuator saturation. These parameters define the trade-off between convergence speed, robustness to noise, and the enforcement of actuator constraints; the next section discusses their practical tuning.

3.1. Dither placement and daylight-convergence criterion

Microalgae raceways exhibit very slow time-varying pH dynamics, and ESC is enabled only during the daylight window. Selecting the dither slower than the dominant bandwidth would yield too few cycles per day to estimate the gradient and converge. Therefore, the dither frequency ω_d is placed outside the process bandwidth, providing a sufficient number of excitation cycles within a day.

Because the plant significantly attenuates the response at ω_d, the demodulated path is scaled to preserve signal-to-noise ratio (using a reference gain D). Phase shift introduced by this choice, and their compensation using high-pass lead and delayed demodulation, are addressed in the next subsections.

Fig. 4 illustrates the identified range of the dominant first-order dynamics obtained from previous studies of the system (Caparroz et al., 2024): the fastest observed time constant is $\tau^- = 420\,\mathrm{s}$ and the slowest is $\tau^+ = 1500\,\mathrm{s}$, corresponding to corner frequencies $\omega_p^+ = 1/\tau^- \approx 2.38{\times}10^{-3}\,\mathrm{rad\,s^{-1}}$ and $\omega_p^- = 1/\tau^+ \approx 6.67{\times}10^{-4}\,\mathrm{rad\,s^{-1}}$. The selected dither is

$$\boxed{\omega_d = 0.0052\ \mathrm{rad\,s^{-1}}} \quad \Rightarrow \quad T_d = \frac{2\pi}{\omega_d} \approx 1208.3\ \mathrm{s}$$

which satisfies $\omega_d > \omega_p^+$ and thus guarantees out-of-band excitation across the entire range.

In practice, ω_d is also chosen to yield a target number of cycles during the daylight interval T_{day}:

$$N_{\mathrm{day}} = \frac{\omega_d\, T_{\mathrm{day}}}{2\pi}.$$

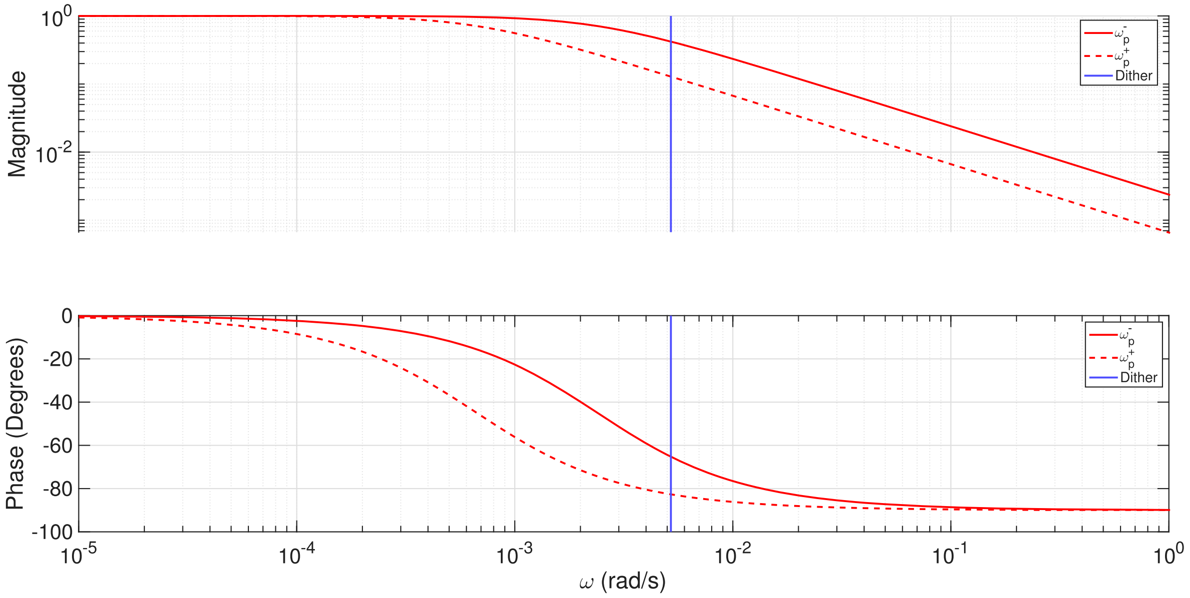

Fig. 4. Magnitude and phase of a first-order plant across the identified range of time constants ($\tau^- = 420\,\mathrm{s}$, $\tau^+ = 1500\,\mathrm{s}$). The vertical line marks the selected dither $\omega_d = 0.0052\ \mathrm{rad\,s^{-1}}$, chosen above to guarantee convergence during the daylight interval.

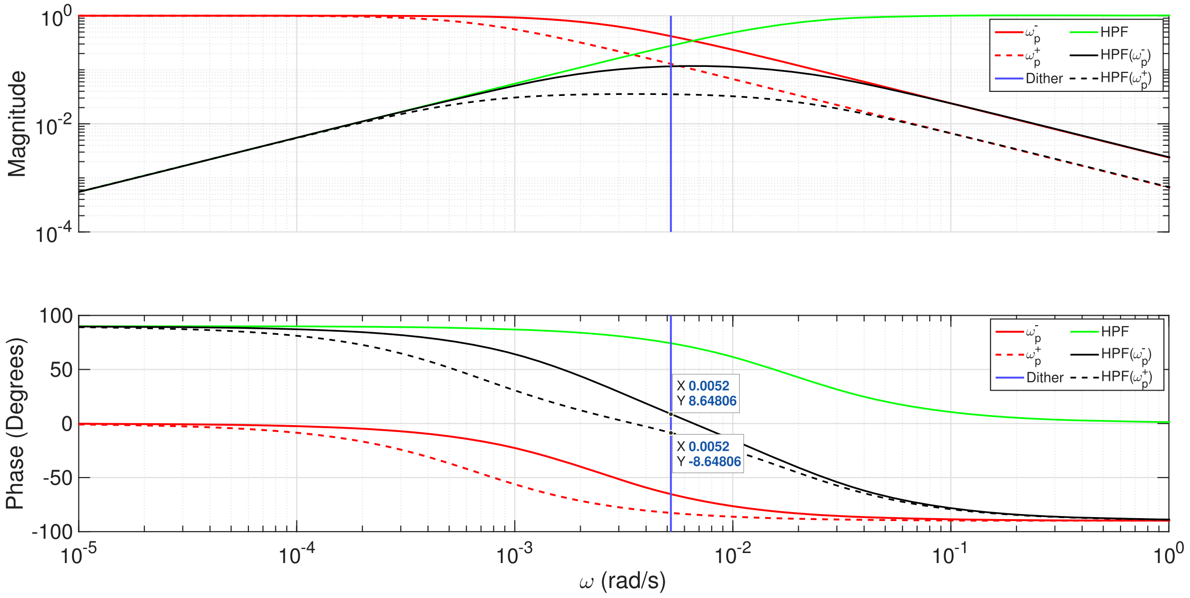

Fig. 5. Design summary at the dither frequency $\omega_d = 0.0052\ \mathrm{rad\,s^{-1}}$. Top: magnitudes of the plant for the fast and slow endpoints ($\omega_p^+ = 1/\tau^-$, $\omega_p^- = 1/\tau^+$), the high-pass filter $HPF(s) = s/(s+\omega_h)$, and the selected ω_d (vertical line). Bottom: phases showing the plant lag (red), the HPF lead (green), and the resulting centered residual (black) at ω_d. The markers indicate the symmetric residual phase $\phi_{\mathrm{rem}}(\omega_d;\omega_p^{\pm},\omega_h) = \pm\Delta\phi$ with $\Delta\phi \approx 8.65°$, obtained with $\omega_h \approx 1.82\times10^{-3}\ \mathrm{rad\,s^{-1}}$. (For interpretation of the references to colour in this figure legend, the reader is referred to the web version of this article.)

For typical daylight windows $T_{\mathrm{day}} \in [6,10]$ h, this gives $N_{\mathrm{day}} \in [17,29]$, ensuring that gradient estimates are well averaged within a single day.

3.2. Phase lag and transport delay

Operating out-of-band introduces a sizable phase lag at the dither frequency ω_d in the plant's dynamic response. This lag is addressed by tuning the washout high-pass filter (HPF) to provide phase lead at ω_d and to center the residual phase over the expected range of plant bandwidths. In addition, the physical layout of the raceway (CO_2 injection at the sump and pH sensing near the end of the loop) produces a *pure transport delay* t_r that is frequency-independent; this delay is compensated by delaying the demodulation reference by $t_d \approx t_r$. The two compensations act on distinct sources of phase and are designed separately such as described below: t_d cancels transport-induced phase, while ω_h shapes the remaining first-order lag.

1. **Washout for drift rejection and phase lead.**
   A first-order high-pass $HPF(s) = \frac{s}{s+\omega_h}$ removes slow drifts and provides phase lead at ω_d. For an approximately first-order plant with cutoff ω_p,

$$\phi_{\mathrm{system}}(\omega_d) = -\arctan\left(\frac{\omega_d}{\omega_p}\right), \qquad \phi_{\mathrm{HPF}}(\omega_d) = \frac{\pi}{2} - \arctan\left(\frac{\omega_d}{\omega_h}\right)$$

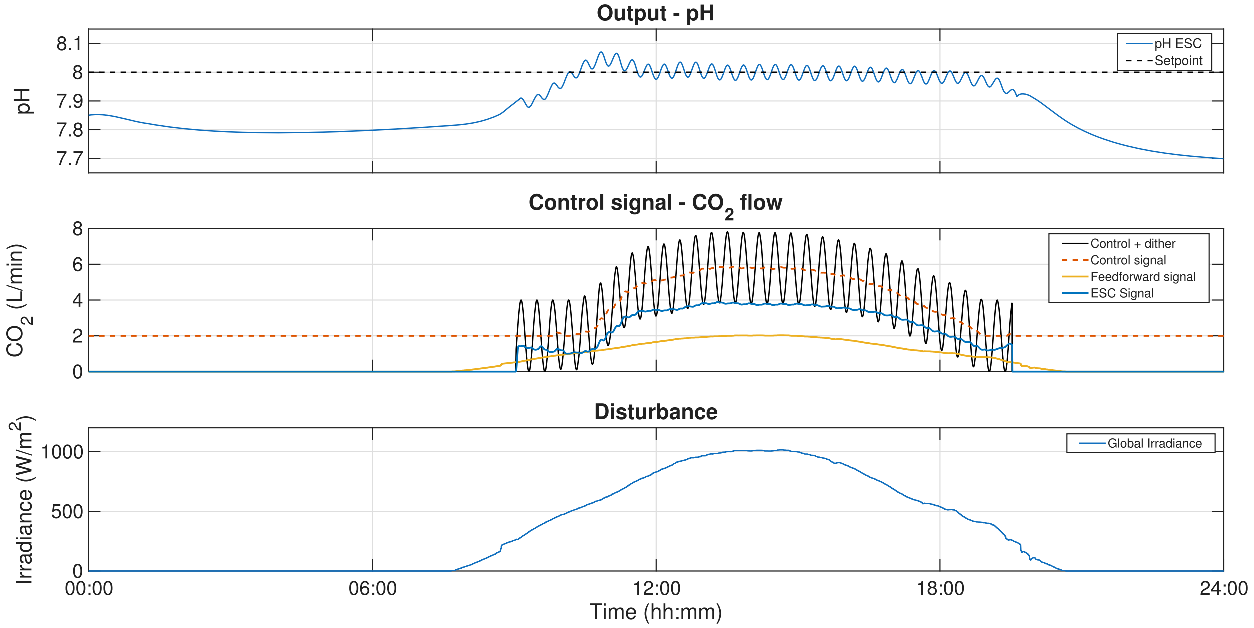

Fig. 6. Simulation clear-sky.

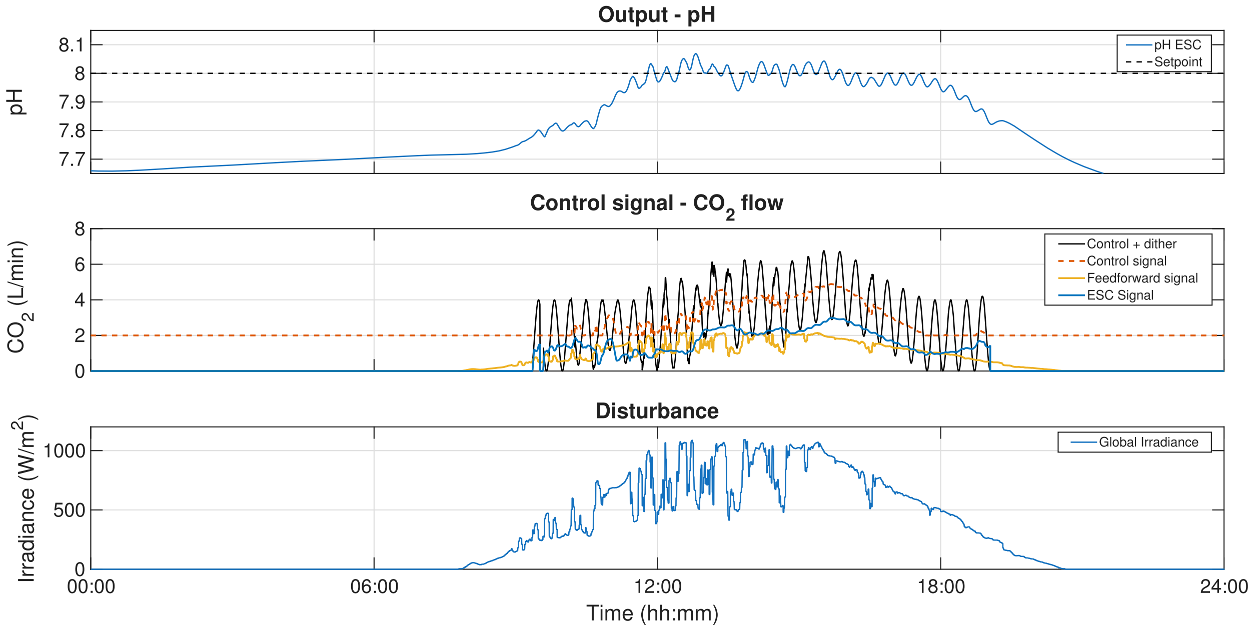

Fig. 7. Simulation cloudy day.

and a practical balance $\phi_{\text{system}} + \phi_{\text{HPF}} \approx 0$ yields the heuristic

$$\omega_h \approx \frac{\omega_d^2}{\omega_p}$$

2. **Demodulator time delay to compensate *transport* delay only.**

The dominant phase lag also includes a *transport delay* t_r set by the reactor layout. This delay is frequency independent and represents the travel time from injection to sensor (e.g.,$t_r \approx L_s/v_{\text{avg}}$), so it contributes $\Phi_{\text{transport}}(\omega_d) = -\omega_d t_r$ to the phase at the dither frequency. To compensate this effect without modifying the amplitude of the demodulating signal or the non-delay dynamics, the demodulator uses a time-delayed copy of the injected dither,

$$Dither_{demod}(t) = G_d \sin\big(\omega_d(t + t_d)\big), \qquad t_d \approx t_r$$

which is equivalent to adding a phase $\varphi_d = \omega_d t_d$ and G_d is a small gain used to fine-tune the demodulating signal amplitude. Both the plant transport delay and the demodulator delay contribute phase terms that are linear in ω_d, with slopes $-t_r$ and $+t_d$, so choosing $t_d \approx t_r$ cancels the transport delay in a neighborhood of the design frequency ω_d. The remaining phase lead required to offset the non-delay plant lag is then provided by the washout filter (Ariyur & Krstić, 2003; Hendrickson & M'Closkey, 2012; Krstić, 2000).

With the transport delay compensated in the demodulation (t_d), the remaining phase to be centered is the sum of the first-order plant lag and the HPF lead:

$$\phi_{\text{rem}}(\omega_d; \omega_p, \omega_h) = \underbrace{-\arctan\left(\frac{\omega_d}{\omega_p}\right)}_{\phi_{\text{system}}(\omega_d)} + \underbrace{\left(\frac{\pi}{2} - \arctan\left(\frac{\omega_d}{\omega_h}\right)\right)}_{\phi_{\text{HPF}}(\omega_d)}.$$

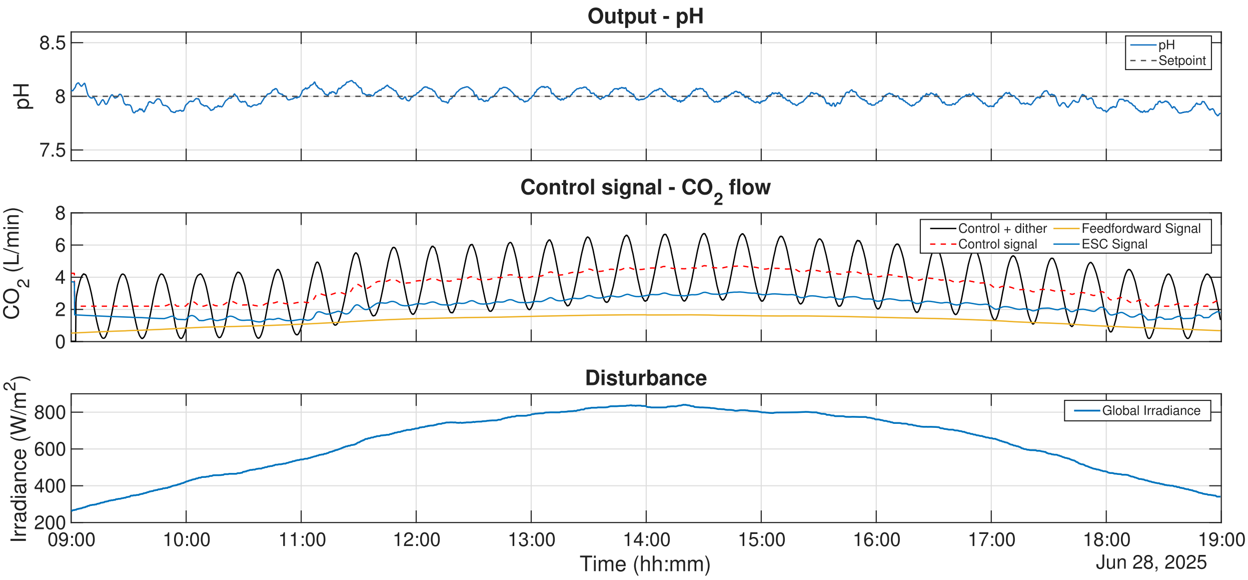

Fig. 8. Performance on the 80 m² raceway (28 June 2025).

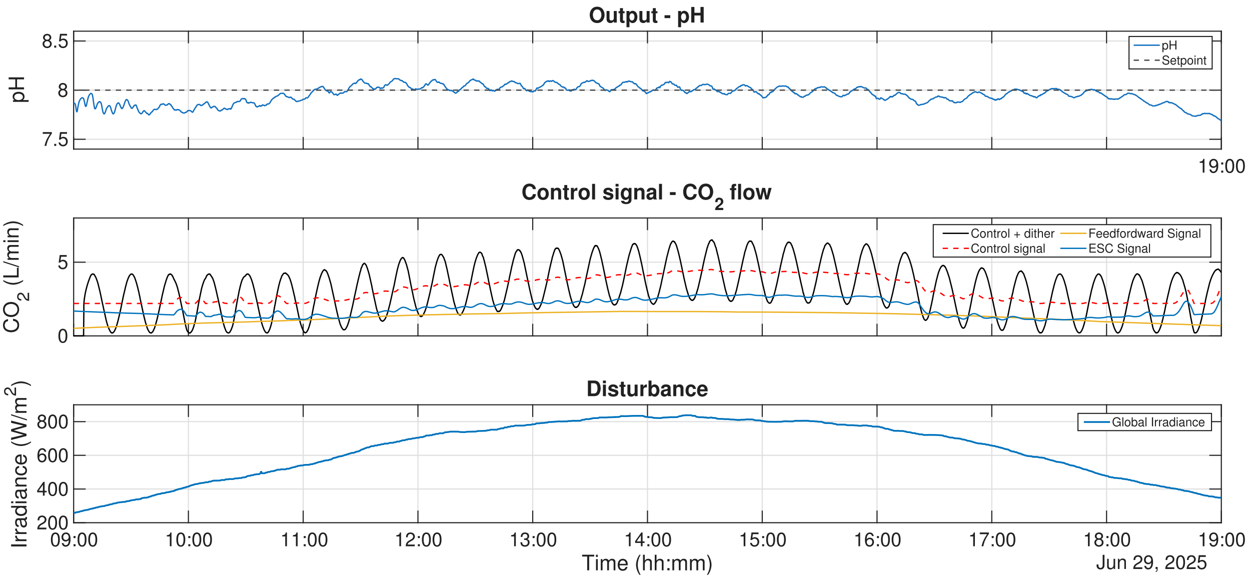

Fig. 9. Performance on the 80 m² raceway (29 June 2025).

Let $\omega_p \in [\omega_p^-, \omega_p^+]$. The HPF cutoff ω_h is chosen to *center* the compensation so that the endpoint residuals are equal and opposite:

$$\phi_{\mathrm{rem}}(\omega_d;\omega_p^-,\omega_h) \;=\; -\phi_{\mathrm{rem}}(\omega_d;\omega_p^+,\omega_h).$$

Writing $\beta \triangleq \arctan\left(\frac{\omega_d}{\omega_h}\right)$, this equal-ripple condition gives

$$\beta \;=\; \frac{\pi}{2} - \frac{1}{2}\left[\arctan\left(\frac{\omega_d}{\omega_p^-}\right) + \arctan\left(\frac{\omega_d}{\omega_p^+}\right)\right], \qquad \omega_h \;=\; \frac{\omega_d}{\tan\beta}$$

Using the identified range $\tau^- = 420$ s and $\tau^+ = 1500$ s (i.e., $\omega_p^+ = 1/\tau^- \approx 2.38\times10^{-3}\ \mathrm{rad\,s^{-1}}$, $\omega_p^- = 1/\tau^+ \approx 6.67\times10^{-4}\ \mathrm{rad\,s^{-1}}$) and the selected dither $\omega_d = 0.0052\ \mathrm{rad\,s^{-1}}$, the centering rule yields

$$\boxed{\omega_h \approx 1.82\times10^{-3}\ \mathrm{rad\,s^{-1}}}$$

The total phase at the dither frequency is expressed as

$$\Phi_{\mathrm{total}}(\omega_d) \;=\; \underbrace{\Phi_{\mathrm{transport}}(\omega_d)}_{\text{canceled by } +\omega_d t_d} \;+\; \underbrace{\Phi_{\mathrm{system}}(\omega_d)}_{\text{first-order lag}} \;+\; \underbrace{\Phi_{\mathrm{HPF}}(\omega_d)}_{\text{lead/centering via } \omega_h}$$

and the design targets a *centered* compensation so that the residual phase error is bounded and approximately symmetric over the expected operating range; in this case,

$$\phi_{\mathrm{rem}}(\omega_d;\omega_p^{\pm},\omega_h) = \pm\Delta\phi \quad \text{with} \quad \boxed{\Delta\phi \approx 8.65^\circ}.$$

These design choices are summarized in Fig. 5. The figure shows the Bode plots of the plant and the HPF together with the selected dither frequency: the top panel compares the magnitudes of the fast and slow plant endpoints and the high-pass filter, while the bottom panel shows the corresponding phases and highlights the symmetric residual phase error $\phi_{\mathrm{rem}}(\omega_d;\omega_p^{\pm},\omega_h) = \pm\Delta\phi$.

The demodulator delay t_d compensates the transport delay t_r and does not enter the HPF centering. It is set directly from the measured transport time, and the corresponding phase rotation is $\varphi_d = \omega_d t_r$:

$$t_d \approx t_r, \qquad \varphi_d = \omega_d t_r.$$

with $\omega_d = 0.0052\ \mathrm{rad\,s^{-1}}$:

$$\boxed{t_r = 360\ \mathrm{s} \;\Rightarrow\; \varphi_d = 1.87\ \mathrm{rad}\ \ (107.26^\circ)}$$

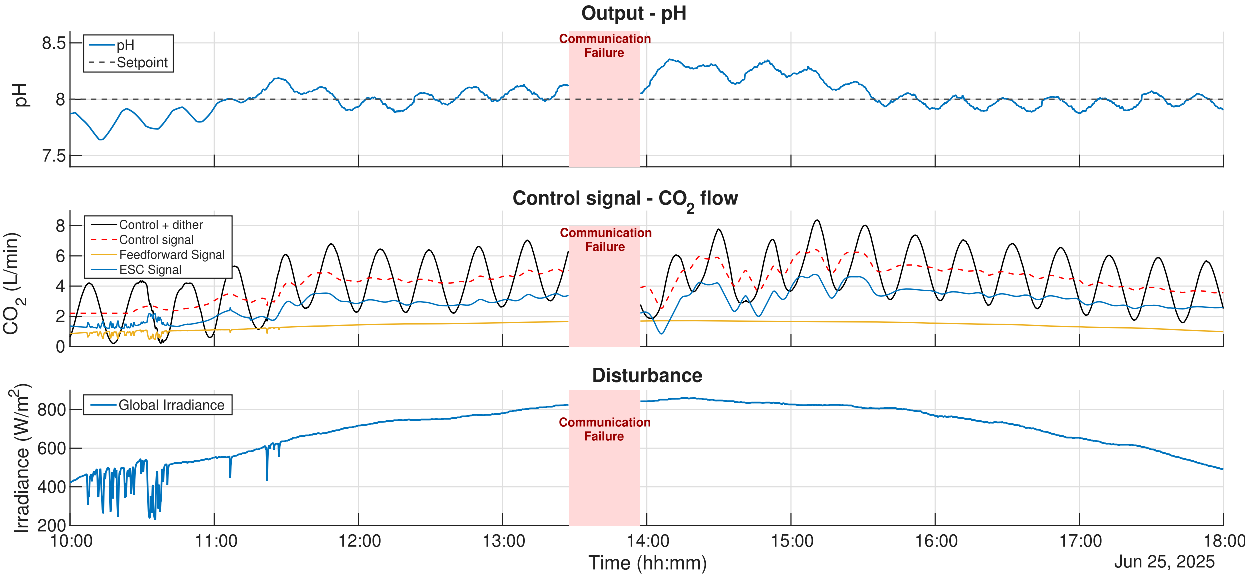

Fig. 10. Controller response during a temporary communication failure.

Table 1
Summary of the parameters used in ESC controller implemented on real raceway.

Parameter	Description	Simulation value	Raceway value	Units
a	Dither amplitude	2	2	L/min
ω_d	Dither angular frequency	0.0052	0.0052	rad/s
ω_h	High-pass filter cutoff angular frequency	0.182	**0.26**	rad/s
k	Integrator gain	1.5	**0.8**	–
k_{ff}	Static Feedforward gain	0.002	0.002	L m^2/W min
ρ	Slew limiter [$\pm a\omega_d$]	± 0.0104	± 0.0104	L/(min s)
G_{aw}	Anti-windup feedback gain	0.05	0.05	–
G_d	Demodulator gain	1.5	**1**	–
t_r	Demodulator delay (transport delay)	360	360	s

3.3. Irradiance feedforward and disturbance rejection

The ESC is responsible for driving the pH toward the local optimum of the cost function, which in this study consists of minimizing the error between the setpoint and the current value, such as expressed in Eq. (9). However, predictable diurnal disturbances due to solar irradiance I_{solar} induce systematic deviations that are better counteracted through feedforward control (Guzmán et al., 2024).

As the control strategy proposed in this work is fundamentally model-free, we incorporate a static data-driven feedforward compensator derived from empirical observations, exploiting the steady-state relationship between pH and irradiance:

$$\Delta V^{\mathrm{ff}}_{CO_2}(t) = -\,\kappa_{\mathrm{ff}}\,\Delta I_{\mathrm{solar}}(t), \tag{10}$$

where $\Delta V^{\mathrm{ff}}_{CO_2}$ represents the incremental control signal provides by the feedforward compensator for an increment in the solar irradiance, $\Delta I_{\mathrm{solar}}(t)$, and κ_{ff} is the static feedforward gain (see Fig. 3).

Following the procedure described in Caparroz et al. (2025b), the κ_{ff} value was estimated experimentally by data observation on the incremental CO_2 flow commanded by a PI controller versus the concurrent increase in irradiance, obtaining a value of

$$\boxed{\kappa_{\mathrm{ff}} = 0.002\,\frac{L\cdot m^2}{W\cdot min}}$$

Thus, irradiance variations are preemptively counteracted by the feedforward compensator, while ESC corrects residual mismatches, slow drifts, and biological changes.

3.4. Final design and discrete-time realization

The flow of CO_2 is physically limited to [0, 12] L/min. To keep the excitation away from the maximum limits and avoid negative flows, saturation with a protection band is applied. These bands are limited by the dither amplitude (a), so that when the control signal is added to the dither, it is bounded within [0, 12] L/min, as follows

$$u_{\mathrm{unsat}}(t) = u_{\mathrm{ESC}}(t) + u_{\mathrm{ff}}(t), \tag{11}$$

$$u_{sat}(t) = \mathrm{sat}_{[\,a,\,12-a\,]}\big(u_{\mathrm{unsat}}(t)\big) \tag{12}$$

where $\mathrm{sat}_{[\,x_{\min},\,x_{\max}\,]}(x)$ represents the saturation of x between $x_{\min}$ and $x_{\max}$.

The raw adaptation driving the integrator includes both the gradient and the anti-windup back-calculation term,

$$\dot{\hat{\theta}}_{\mathrm{raw}}(t) = k\,\zeta(t) \;+\; G_{\mathrm{aw}}\,\underbrace{\big(u_{sat}(t) - u_{\mathrm{unsat}}(t)\big)}_{e_{\mathrm{sat}}(t)}$$

where k and G_{aw} are tuned according to the values in Table 1.

To prevent the adaptation from “chasing” the carrier and to keep the anti-windup correction from producing excessively fast updates, the integrator input is slew-limited to the dither’s maximum slope:

$$\rho \;\triangleq\; a\,\omega_d, \qquad \dot{\hat{\theta}}(t) = \mathrm{sat}_{[-\rho,\rho]}\big(\dot{\hat{\theta}}_{\mathrm{raw}}(t)\big), \qquad \hat{\theta}(t) = \int_0^t \dot{\hat{\theta}}(\tau)\,d\tau \tag{13}$$

A tracking state drives the command toward the saturated output, avoiding integral windup:

$$\dot{x}_{\mathrm{aw}}(t) = G_{\mathrm{aw}}\,[\,u_{sat}(t) - u_{\mathrm{unsat}}(t)\,], \qquad G_{\mathrm{aw}} > 0 \tag{14}$$

When the actuator saturates within the guard band $[a, 12{-}a]$,x_{aw} compensates the saturation error so that it does not accumulate.

Since the ESC is only enabled during the day, when the sun sets, the CO_2 flow is deactivated until the following sunrise and the integrator is reset to eliminate the accumulated action.

The controller is executed digitally in MATLAB at the real facilities as a periodic script that exchanges process tags with the plant PLCs via OPC (read: pH, irradiance, flows; write: CO_2 flow setpoint). Two practical consequences follow. *First*, a first-order high-pass in discrete time (e.g., ZOH-discretized $H(z)$) removes drift but does not reproduce the continuous-time phase lead at ω_d. Therefore, the demodulation reference is given an extra phase shift so that it compensates *both* the plant transport delay and the lead that the washout would provide in continuous time:

$$\begin{aligned} Dither_{demod}[n] &= \sin\big(\omega_d\,(nT_s - t_d^{\star})\big), \\ t_d^{\star} &\approx t_r + t_{\text{lead}} \end{aligned}$$

where n is the sampling instant, T_s is the sampling time, and t_{lead} is the continuous-time phase lead at ω_d in seconds. *Second*, a short warm-up is enforced before enabling adaptation: once irradiance exceeds a small threshold, the dither is injected and the washout/demodulation run for 2 dither periods while control action remains disabled; thereafter the ESC update is enabled. This allows filter states to settle and the gradient estimate to stabilize under daylight operation. The MATLAB script handles daytime gating and time-stamping.

4. Results

This section summarizes first a simulation study that evaluates controller design and tuning insights, and secondly experimental validation on the 80 m^2 outdoor raceway described in Section 2.2. As commented above, the proposed ESC scheme was implemented and evaluated in a physics-based raceway simulator in a first stage, enabling safe tuning and diagnosis under representative diurnal forcing and actuator limits. Once validated in simulation, the same controller architecture with fine-tuning are deployed on a single 80 m^2 outdoor raceway at the CIESOL research facility (Almería, Spain), demonstrating correct operation beyond simulations and confirming effectiveness under real operating conditions.

The ESC architecture in Fig. 3 was first implemented in the raceway simulator to validate the controller structure and perform preliminary tuning (see Table 1), demonstrating closed-loop convergence and confirming that the scheme can be deployed on the real reactor safely. Figs. 6–7 show closed-loop simulations driven by measured irradiance for two representative clear-sky day and one cloudy day. Each figure reports: (top) the pH output and its setpoint; (middle) the $\mathrm{CO_2}$ flow, decomposed into the irradiance feedforward contribution, the ESC signal, and their sum including the dither; and (bottom) the global irradiance disturbance.

Under clear-sky irradiance (Fig. 6), the closed loop converges rapidly from the initial morning conditions and tracks the pH setpoint within a narrow band, while the $\mathrm{CO_2}$ flow follows the daily irradiance profile: the feedforward term provides the slow baseline and the ESC adds the high-frequency modulation required for extremum seeking. For the cloudy day (Fig. 7), the irradiance exhibits strong short-term variability, yet the pH convergence remains fast and setpoint tracking is preserved. In this case the feedforward path responds to the low-frequency envelope of the disturbance, whereas the ESC loop compensates the residual mismatch. These results confirm that the selected tuning achieves the intended trade-off between convergence speed and robustness prior to experiments on the real reactor.

Once correct operation had been verified in simulation (driven by measured irradiance and operating data), the ESC was deployed on the real 80 m^2 raceway to confirm performance under field conditions. The implementation mirrored the simulated ESC architecture, while the controller parameters were slightly re-tuned to account for the modest mismatch between the reactor and its dynamic model (see Table 1). In particular, the integrator gain k and demodulation gain G_d values were reduced from 1.5 to 0.8 and from 1.5 to 1, respectively, making the ESC control signal less aggressive. Moreover, the high-pass cutoff was increased from $\omega_h = 0.182$ rad/s in simulation to $\omega_h = 0.26$ rad/s on the real plant, providing a slightly faster washout that more strongly attenuates the low-frequency drift and measurement noise observed in the reactor but absent from the simulator, without changing the qualitative ESC behaviour.

A further practical modification concerned the actuator lower bound: the $\mathrm{CO_2}$ flow was constrained to a minimum of 0.2 L/min. This choice is motivated by the fact that near-zero flows exhibit nonlinearity and stick-slip behaviour, which can distort the lower lobe of the injected dither and inject harmonics that bias demodulation. Imposing a 0.2 L/min minimum prevents this distortion; owing to its small magnitude relative to the operating range, this constraint has negligible impact on the overall $\mathrm{CO_2}$ delivery and regulation objectives

After enabling the algorithm on site, day-long runs were conducted. The results reported in Figs. 8–9 illustrate the startup sequence: following the irradiance threshold, the dither is injected while adaptation remains disabled for a two-period warm-up. During this interval, the pH shows transient oscillations associated with $\mathrm{CO_2}$ recirculation and filter state settling; once stabilized, the dither component becomes clearly visible in pH and the ESC update is enabled, yielding consistent convergence toward the setpoint despite diurnal disturbances.

The pH remains close to the setpoint for most of the daylight interval, with a bounded ripple at the dither period and small tracking drifts following the slow decay of irradiance. The control decomposition clarifies the roles: the *feedforward* (orange) follows the diurnal radiation profile, providing the dominant baseline; the *ESC signal* (blue) adds a slower corrective bias that keeps pH centered; and their sum (red dashed) is the control signal. The black trace (sum + dither) preserves a nearly constant sinusoidal amplitude across the day, indicating slew-limiting prevents the adaptation from chasing the carrier.

Fig. 10 shows a shaded interval that corresponds to a loss of communication with the PLC. During this outage, the pH is not read and no control command reaches the actuator; the dither disappears and the CO_2 flow no longer tracks the ESC/FF signal, leading to a radiation-driven increase in pH. After reconnection, the dither reappears and the control signal resumes tracking, bringing pH back toward the setpoint. This clearly shows that the ESC generated signal is coherent and achieves within-day convergence, even after a disconnection has driven the pH away from the region where the static feedforward alone maintains regulation.

5. Conclusions

This work has demonstrated that a classical modulation-demodulation ESC, purposely tailored for daylight operation with an out-of-band dither, is an effective and practical solution for pH regulation in raceway photobioreactors. The key design elements were selecting the dither above the process bandwidth to secure sufficient cycles per day, using a washout tuned for phase lead/centering at the dither frequency, compensating the transport delay by delaying the demodulation reference, and including a static irradiance feedforward. All these elements were validated from analysis to practice. A discrete-time realization with guard-banded saturation, anti-windup, slew-limited adaptation, daytime gating, and a short warm-up ensures robust behaviour on real equipment.

In simulations (clear and cloudy days) and in outdoor trials, the closed-loop converged rapidly during daylight, maintained the pH setpoint with bounded ripple at the carrier period, and recovered gracefully from a temporary loss of communications without retuning. The method required minimal modeling effort, tolerated slow biological drift, and preserved the integrity of the demodulation despite actuator limits and measurement delays. Together, these results position ESC as a low-complexity, model-free tool for real-time operation near the pH that supports high productivity in large-scale raceways Table A.1.

Future work will target cost functions directly tied to productivity by leveraging online estimates of biomass concentration, so that ESC optimizes a production proxy rather than a quadratic penalty around a pH setpoint. In parallel, we will implement automatic adaptation of the demodulation delay as the culture velocity changes, either from a liquid-velocity sensor or inferred from the paddle-wheel speed commanded by the variable-frequency drive, thereby maintaining proper phase alignment as recirculation conditions evolve. Finally, we are currently conducting trials on larger industrial-scale raceway photobioreactors to assess scalability, robustness, and adaptation throughout full, real cultivation campaigns.

CRediT authorship contribution statement

José González-Hernández: Writing – review & editing, Writing – original draft, Visualization, Validation, Methodology, Investigation, Formal analysis, Data curation; **Laurent Dewasme:** Writing – review & editing, Supervision, Formal analysis; **José Luis Guzmán:** Writing – review & editing, Supervision, Investigation, Formal analysis; **José Carlos Moreno:** Writing – review & editing, Supervision, Investigation; **Alain Vande Wouwer:** Writing – review & editing, Investigation, Formal analysis.

Declaration of competing interest

The authors declare that they have no known competing financial interests or personal relationships that could have appeared to influence the work reported in this paper.

Acknowledgement

This work has been partially funded bythe following projects [grant numbers PID2023-150739OB-I00] funded by the Spanish Ministry of Science and the European Union (grant agreement ID: 101060991, REALM).

Appendix A. Simulation model parameters

Table A.1
Parameters and variables used in Models (1)–(4).

Symbol	Description	Units
μ	Overall specific growth rate	d^{-1}
$\mu(I_{av})$	Maximum specific growth rate as a function of mean irradiance	d^{-1}
$\mu(T)$	Temperature normalization factor	–
$\mu(\mathrm{pH})$	pH normalization factor	–
$\mu(O_2)$	Oxygen normalization factor	–
m	Maintenance/respiration term	d^{-1}
d_r	Dilution rate term	d^{-1}
Q_d	Dilution flow	$m^3\,s^{-1}$
V_r	Reactor volume	m^3
C_b	Biomass concentration	$kg\,m^{-3}$
$[O_2]$, $[O_2]^\star$	Dissolved oxygen concentration and equilibrium concentration	$mol\,m^{-3}$
$[O_2]^{iny}$	Equivalent DO at injection	$mol\,m^{-3}$
$[CO_2]$, $[CO_2]^\star$	Dissolved CO_2 concentration and equilibrium concentration	$mol\,m^{-3}$
$[CO_2]^{iny}$	Equivalent CO_2 at injection	$mol\,m^{-3}$
C_T	Total inorganic carbon	$mol\,m^{-3}$
$[C_T]_{in}$	Inlet total inorganic carbon concentration	$mol\,m^{-3}$
Y_{O_2}	Oxygen yield coefficient	–
M_{O_2}	Molar mass of O_2	$kg\,mol^{-1}$
Y_{CO_2}	CO_2 yield coefficient	–
M_{CO_2}	Molar mass of CO_2	$kg\,mol^{-1}$
k^{atm}_{La,O_2}	Volumetric mass transfer coefficient (O_2, air–water)	s^{-1}
k_{La,O_2}	Volumetric mass transfer coefficient (O_2, injection)	s^{-1}
k^{atm}_{La,CO_2}	Volumetric mass transfer coefficient (CO_2, air–water)	s^{-1}
kL_{La,CO_2}	Volumetric mass transfer coefficient (CO_2, injection)	s^{-1}

References

Acién, F. G., Fernández, J. M., Magán, J. J., & Molina, E. (2012). Production cost of a real microalgae production plant and strategies to reduce it. *Biotechnology Advances*, *30*(6), 1344–1353. Special issue on ACB 2011. https://doi.org/10.1016/j.biotechadv.2012.02.005

Acién, F. G., Molina, E., Reis, A., Torzillo, G., Zittelli, G. C., Sepúlveda, C., & Masojídek, J. (2017). Photobioreactors for the production of microalgae. In C. Gonzalez-Fernandez, & R. Muñoz (Eds.), *Microalgae-based biofuels and bioproducts* Woodhead Publishing Series in Energy (pp. 1–44). Woodhead Publishing. https://doi.org/10.1016/B978-0-08-101023-5.00001-7

Ariyur, K. B., & Krstić, M. (2003). Real-time optimization by extremum-seeking control. Hoboken, NJ: Wiley-Interscience. https://doi.org/10.1002/0471669784

Caparroz, M., Guzmán, J. L., Berenguel, M., & Acién, G. (2024). A novel data-driven model for prediction and adaptive control of pH in raceway reactor for microalgae cultivation. *New Biotechnology*, *82*. https://doi.org/10.1016/j.nbt.2024.04.001

Caparroz, M., Guzmán, J. L., Gil, J. D., Berenguel, M., & Acién, F. G. (2025a). A hybrid MRAC-PI approach to regulate pH in raceway reactors for microalgae production. *Control Engineering Practice*, *156*, 106191. https://doi.org/10.1016/j.conengprac.2024.106191

Caparroz, M., Soltesz, K., Hägglund, T., Guzmán, J. L., & Berenguel, M. (2025b). A new approach to relay-based autotuning PID controllers and their evaluation in pH control of industrial photobioreactors. *Control Engineering Practice*, *164*, 106520. https://doi.org/10.1016/j.conengprac.2025.106520

Carreño Zagarra, J., Guzmán, J. L., Moreno, J. C., & Villamizar, R. (2019). Linear active disturbance rejection control for a raceway photobioreactor. *Control Engineering Practice*, *85*, 271–279. https://doi.org/10.1016/j.conengprac.2019.02.007

Dewasme, L., & Vande Wouwer, A. (2020). Model-free extremum seeking control of bioprocesses: A review with a worked example. *Processes*, *8*(10), 1209. https://doi.org/10.3390/pr8101209

Feudjio Letchindjio, C. G., Dewasme, L., Deschênes, J.-S., & Vande Wouwer, A. (2019). An extremum seeking strategy based on block-oriented models: Application to biomass productivity maximization in microalgae cultures. *Industrial & Engineering Chemistry Research*, *58*(30), 13481–13494. https://doi.org/10.1021/acs.iecr.9b00667

Feudjio Letchindjio, C. G., Dewasme, L., & Vande Wouwer, A. (2021). An experimental application of extremum seeking control to cultures of the microalgae scenedesmus obliquus in a continuous photobioreactor. *International Journal of Adaptive Control and Signal Processing*, *35*(7), 1285–1297. https://doi.org/10.1002/acs.3196

González-Hernández, J., Rodríguez-Miranda, E., Guzmán, J. L., Acién Fernández, F. G., & Visioli, A. (2022). Optimización de temperatura en reactores raceway para la producción de microalgas mediante regulación de nivel. *Revista Iberoamericana de Automática e Informática Industrial*, *19*, 164-173. https://doi.org/10.4995/riai.2022.16586

Guzmán, J. L., Berenguel, M., Rodríguez-Miranda, E., & Acién, F. G. (2025). Microalgae production at industrial scale: Modelling and control challenges. In *American control conference 2025 (ACC25), denver (USA), july 8–10*. https://doi.org/10.23919/ACC63710.2025.11107686

Guzmán, J. L., Hägglund, T., de Gruyter, G., & Co, K. G. W. (2024). Feedforward control: Analysis, design, tuning rules, and implementation. De Gruyter Textbook Series. De Gruyter. https://doi.org/10.1515/9783111429489

Hendrickson, C., & M'Closkey, R. T. (2012). Phase compensation strategies for modulated–demodulated control with application to pulsed jet injection. *Journal of Dynamic Systems, Measurement, and Control*, *134*(1), 011024. https://doi.org/10.1115/1.4005081

Johnson, D. A., Weissman, J., & Goebel, R. (1988). An outdoor test facility for the large-scale production of microalgae. Solar Energy Research Inst., Golden, CO (USA); Microbial Products, Inc., Fairfield, CA (USA). https://www.osti.gov/biblio/5068121.

Krstić, M. (2000). Performance improvement and limitations in extremum seeking control. *Systems & Control Letters*, *39*(5), 313–326. https://doi.org/10.1016/S0167-6911(99)00111-5

Krstić, M., & Wang, H. (2000). Stability of extremum seeking feedback for general nonlinear dynamic systems. *Automatica*, *36*(4), 595–601. https://doi.org/10.1016/S0005-1098(99)00183-1

Lara, J. M. Z., Dewasme, L., & Vande Wouwer, A. (2025). A cheap real-time optimal control setup for microalgae cultures: Simulation and experimental results. *Biochemical Engineering Journal*, (p. 109833). https://doi.org/10.1016/j.bej.2025.109833

Nordio, R., Delgado, F., Sánchez-Zurano, A., González-Hernández, J., Rodríguez-Miranda, E., Guzmán, J. L., Lafarga, T., & Acién, G. (2022). Long-term assessment of the nutrient recovery capacity and biomass productivity of scenedesmus almeriensis in raceway reactors using unprocessed urban wastewater. *Bioresource Technology*, *369*, 128374. https://doi.org/10.1016/j.biortech.2022.128374

Otálora, P., Banerjee, S., Mistiri, M. E., Khan, O., Rivera, D. E., & Guzmán, J. L. (2026). Enhancing pH control in microalgae raceway photobioreactors using 3DoF-KF model-on-demand model predictive control. *Control Engineering Practice*, *168*, 106742. https://doi.org/https://doi.org/10.1016/j.conengprac.2025.106742

Pataro, I. M. L., Gil, J. D., Guzmán, J. L., Berenguel, M., & Lemos, J. M. (2023). A learning-based model predictive strategy for pH control in raceway photobioreactors with freshwater and wastewater cultivation media. *Control Engineering Practice*, *138*, 105619. https://doi.org/10.1016/j.conengprac.2023.105619

Pawlowski, A., Guzmán, J. L., Berenguel, M., & Acién, F. G. (2019). Control system for pH in raceway photobioreactors based on wiener models. *IFAC-PapersOnLine*, *52*(1), 928–933. 12th IFAC Symposium on Dynamics and Control of Process Systems, including Biosystems DYCOPS 2019. https://doi.org/10.1016/j.ifacol.2019.06.181

Rodríguez Miranda, E., Guzman, J. L., Acién Fernandez, F. G., & Berenguel, M. (2025). A comprehensive dynamic model of microalgae production in open raceway systems. Version available on Zenodo https://doi.org/10.5281/zenodo.15579693

Rodríguez-Miranda, E., Beschi, M., Guzmán, J. L., Berenguel, M., & Visioli, A. (2019). Daytime/nighttime event-based PI control for the pH of a microalgae raceway reactor. *Processes*, *7*(5). https://doi.org/10.3390/pr7050247

Rodríguez-Miranda, E., Guzmán, J. L., Berenguel, M., Acién, F. G., & Visioli, A. (2020). Diurnal and nocturnal pH control in microalgae raceway reactors by combining classical and event-based control approaches. *Water Science and Technology*, *82*(6), 1155–1165. https://doi.org/10.2166/wst.2020.260

Rodríguez-Miranda, E., Otálora, P., González-Hernández, J., Guzmán, J. L., & Berenguel, M. (2025). A comprehensive benchmark platform for process control research of outdoor microalgae raceway reactors. https://arxiv.org/abs/2512.15916.

Sánchez-Zurano, A., Rodríguez-Miranda, E., Guzmán, J. L., Acién-Fernández, F. G., Fernández-Sevilla, J. M., & Molina Grima, E. (2021). ABACO: A new model of microalgae-bacteria consortia for biological treatment of wastewaters. *Applied Sciences*, *11*(3), 998. https://doi.org/10.3390/app11030998

Tan, Y., Nešić, D., & Mareels, I. (2006). On non-local stability properties of extremum seeking control. *Automatica*, *42*(6), 889–903. https://doi.org/10.1016/j.automatica.2006.01.014

Tapie, P., & Bernard, A. (1988). Microalgae production: Technical and economic evaluations. *Biotechnology and Bioengineering*, *32*(7), 873–885. https://doi.org/10.1002/bit.260320705